PHYSICAL REVIEW B

CONDENSED MATTER

THIRD SERIES, VOLUME 44, NUMBER 15 15 OCTOBER 1991-I

Calculation of ground-state and optical properties of boron nitrides in the hexagonal, cubic, and wurtzite structures

Yong-Nian Xu and W. Y. Ching

Department of Physics, University of Missouri-Kansas City, Kansas City, Missouri 64110

(Received 11 March 1991)

The electronic structures, the charge-density distribution, and the total energies of boron nitrides (BN) in the hexagonal, cubic, and wurtzite structures are studied by first-principles self-consistent local-density calculations. For the ground-state properties, the band structures, the equilibrium lattice constants, the bulk modulus and their derivatives, and the cohesive energy are in good agreement with other recent calculations and with experimental data. The relative stabilities and possible phase transitions among these three phases are discussed. The linear optical properties of these three crystals are also calculated and compared with the available measurements. For hexagonal BN, all the structures in the electron-energy-loss function as measured by inelastic electron scattering have been reproduced by the calculation. For cubic BN, the calculated dielectric functions is also in good agreement with the reflectance data. For wurtzite-structure BN, no optical data are available for comparison. These results are discussed in the context of crystal structure and bonding in these three crystals. Based on the analysis of the calculated and measured optical data on cubic and hexagonal BN, it is argued that the assessment of the accuracy of the conduction-band states should rely mainly on the reproduction of major structures in the optical-absorption curves rather than on the size of the band gap. The accuracy of the higher conduction-band states as calculated by the local-density theory is strongly energy and momentum dependent. Furthermore, a determination of the optical gap is complicated by the different roles of the direct and indirect transitions, and by the difficult task of extrapolating data to the low-frequency region.

I. INTRODUCTION

In recent years, the properties of boron nitrides (BN) have been studied in great detail, both theoretically and experimentally. This is mainly due to some of the fascinating properties of BN, such as extreme hardness, high melting point, low dielectric constant, large band gap, etc., that have many applications in modern microelectronic devices and its usefulness as a protective coating material.[1] BN emerged as a very strong competitor with diamond and SiC as far as high-temperature applications are concerned. Also, BN is the lightest III-V compound isoelectronic with the III-V semiconductors such as GaAs, yet with far different properties. BN exists in three crystalline forms.[2] The hexagonal form (h-BN) which is isostructural with graphite is the normal phase stable at room temperature and pressure.[3] The cubic phase (c-BN) (zinc-blende structure) has been synthesized in the laboratory under pressure.[4,5] At a high temperature and pressure, h-BN may transform into a wurtzite structure[6,7] (w-BN) which is the stable structure for AlN. Amorphous BN may also exist[8] in thin films prepared by chemical vapor deposition[9] (CVD) or by sputter deposition.[10]

There have been many studies on the electronic and structural properties of h-BN and c-BN, but relatively few for w-BN.[11–36] Early studies show vastly different results mainly because of deficiencies in the computational methods. In recent years, first-principles calculations in the local-density approximation (LDA) have provided much better and consistent results. These include the LCAO (linear combination of atomic orbitals) calculations with numerical basis by Zunger and Freeman;[23] LCAO–Hartree-Fock study by Dovesi, Pisani, and Roetti;[25] calculations by Huang and Ching;[27] first-principles pseudopotential calculations by Wentzcovitch and coworkers,[30–32,35] and also by Van Camp, Van Doren, and Devresse. Park, Terakura, and Hamada studied the band

structures and the equilibrium lattice constants of all three phases of BN using the full-potential linear-augmented-plane-wave method (FLAPW).[28] Catellani *et al.* used the same method to study the surface and bulk electronic structures of *h*-BN.[29] Takahashi *et al.* calculated the band structure of *c*-BN using the variational cellular method.[34] Wentzcovitch and co-workers carried out probably the most detailed and careful study of the electronic structure and the energetics of possible paths of phase transitions using a pseudopotential mixed-basis approach.[35] The equation of state for *c*-BN was accurate determined both experimentally and theoretically.[36] Very recently, Estreicher, Chu, and Marynick studied the equilibrium structure of a neutral interstitial H in *c*-BN using a cluster-type approach.[37] These studies have greatly advanced our understanding of the electronic and structural properties of BN. There have been several experimental studies on *h*-BN.[38] Recently, measurements have also been made on BN films grown in many different phases.[1] Of particular interest are the inelastic-electron-scattering experiment on *h*-BN by Tarrio and Schnatterly (TS),[39] and the reflectance measurement on *c*-BN by Miyata and Moriki[40] and Osaka *et al.*[9] Indeed, it is these recent optical measurements that have motivated our present investigation on the three phases of BN using the orthogonalized LCAO (OLCAO) method. It turns out that there is an excellent agreement between our calculation and these recent measurements.

In this paper, we report the results of a detailed study on the electronic structure and the optical properties of these three phases of BN. Our calculated band structures and ground-state properties are generally comparable to other recent first-principles LDA calculations using different computational methods. Direct calculation of optical properties based on band-structure results greatly facilitates the interpretation of the experimental data, which in turn provide a deeper understanding of the electronic structures. Detailed analysis of the valence charge distribution brings additional insight into the bonding in different phases of BN.

Since our method of calculation is quite well established and amply documented in earlier publications,[41] it will not be repeated here. The *ab initio* self-consistent OLCAO method has been successfully applied to the study of bulk properties of Si,[42,43] AlN,[44] and SiO_2 crystals[45] by means of total energy (TE) calculations. Recently, the optical properties of many complex inorganic crystals have also been studied.[46–52] The results were generally in good agreement with the experimental data up to very high photon energies.

In the next section, Sec. II, we present the results on the electronic structures and ground-state properties of the three phases of BN. We compare our results with other existing calculations and experimental data. In Sec. III the calculated optical results are compared with recent experiments. The results are further discussed in the last section with a brief conclusion at the end.

II. GROUND-STATE PROPERTIES

A. Band structure and density of states

The band structure of BN is calculated self-consistently using the OLCAO method. A full basis set including the empty $3s$ and $3p$ atomic orbitals of both B and N is employed. Each atomic function is expanded in terms of Gaussian orbitals with decay exponents ranging from 0.15 to 5×10^4. The crystal potential and the charge density are each represented by a sum of atom-centered Gaussian functions of varying exponents. The Wigner interpolation formula is used to account for the correlation effect. The crystal parameters used in the calculation and the key interatomic distances are listed in Table I. Twelve **k** points in the irreducible part of the Brillouin zone (BZ) are used for self-consistent iterations in all three cases. The numerical accuracy achieved in these calculations is adequate and is comparable to similar calculations for other crystals.[43–52]

TABLE I. Crystal structure data of BN.

	Cubic	Wurtzite	Hexagonal
Lattice		$a=2.536$	$a=2.494$
constant (Å)	$a=3.615$	$c=4.199$	$c=6.66$
Volume/molecule (Å^3)	11.810	11.692	17.940
Density (g/cm^3)	3.450	3.485	2.271
Space group	T_d	C_{6v}	D_{6h}
B-N distance (Å)	1.565(4)	1.555(3)	1.440(3)(intralayer)
	2.997(12)	1.575(1)	2.880(3)(intralayer)
	3.939(12)	2.624(1)	3.330(2)(interlayer)
		2.975(3)	3.810(6)(intralayer)
		2.985(6)	
		3.649(6)	
		3.909(6)	
		3.955(3)	
B-B or N-N	2.556(12)	2.536(6)	2.494(6)(intralayer)
distance (Å)	3.615(6)	2.560(6)	2.628(6)(interlayer)
		3.606(6)	

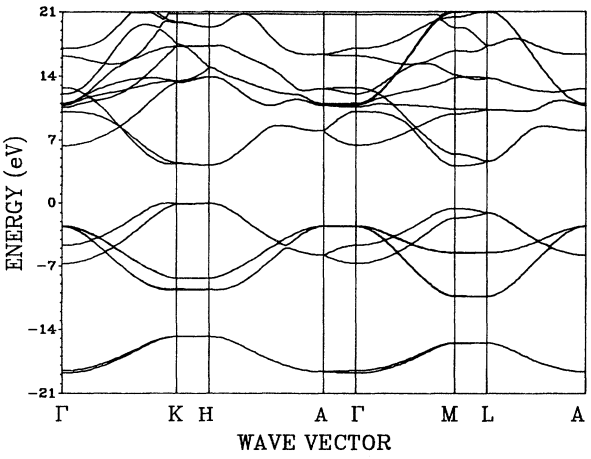

FIG. 1. Calculated band structure of hexagonal BN.

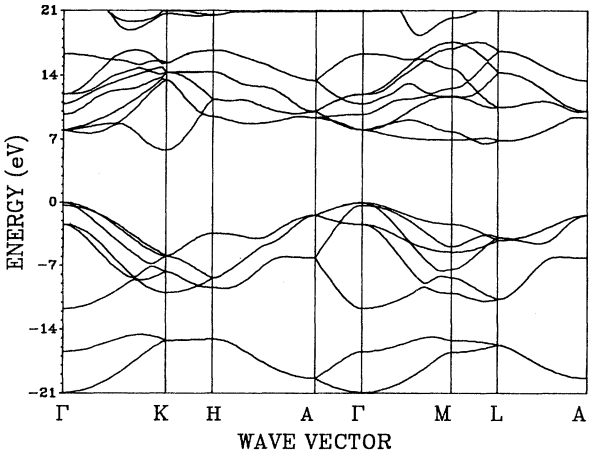

FIG. 3. Calculated band structure of wurtzite BN.

The calculated band structures for h-BN, c-BN, and w-BN are shown in Figs. 1–3, respectively. The corresponding density of states (DOS) and the atom-resolved partial DOS (PDOS) are shown in Figs. 4–6. There are substantial differences in the band structures of h-BN and c-BN and to a lesser extent between c-BN and w-BN. In h-BN, the bonding configuration of the valence electron is sp^2 while in c-BN or w-BN it is sp^3. The graphitelike layer structure of h-BN is reflected in the relatively flat bands along the k_z direction. The calculated band gaps for all three crystals are indirect and have values of 4.07, 5.18, and 5.81 eV for h-BN, c-BN, and w-BN, respectively. The corresponding positions of band extremes are at

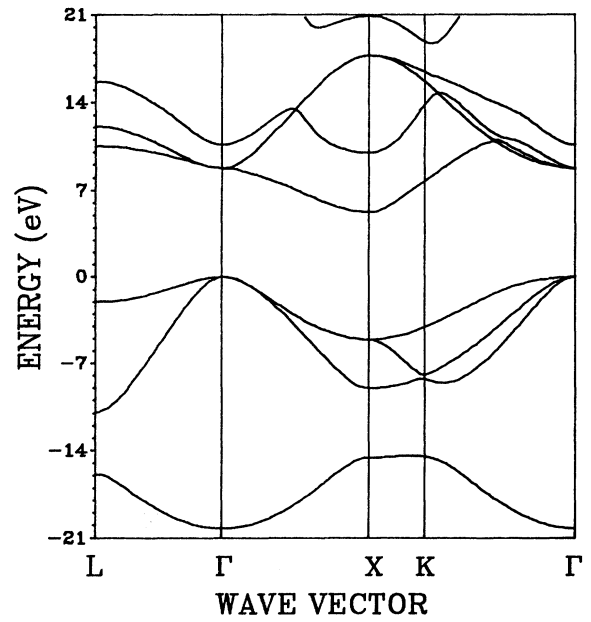

FIG. 2. Calculated band structure of cubic BN.

H, Γ, and Γ for the top of the valence band (VB) and at M, X, and K for the bottom of the conduction band (CB). The direct band gaps in c-BN and w-BN are much larger than the indirect gaps. For h-BN, the two gaps are quite close. These gap values are listed in Table II and they are close to other recent calculations.[28,29,34,35] The calculated indirect gaps are smaller than the reported experimental gaps, and this has often been attributed to the failure of LDA to correctly reproduce the excited states, i.e., the CB. We will return to this point later in discussing the optical results. We find the gap value increases as the volume decreases, a behavior similar to diamond and in agreement with the pseudopotential calculation of Ref. 33. For w-BN, the calculated band structure should be compared with that of AlN calculated using the same method.[44] The general features of the VB are quite similar. AlN has a smaller gap (direct at Γ) and a much narrower VB width of about 6 eV which may indicate a more ionic bonding character in AlN. Apparently, being in the same row of the Periodic Table, B and N are more covalently bonded.

The effective mass (EM) components for electrons and holes along the principal **k** directions for the three crystals are also listed in Table II. As can be expected, the EM for h-BN are highly anisotropic with average in-plane components a factor of 5 smaller than the components perpendicular to the plane. Along the Γ to M direction, the electron and hole EM components are 0.26 and -0.50, respectively, thus the charge carriers in the basal plane of h-BN can be quite mobile. Surprisingly, the EM's for c-BN are also quite anisotropic. For w-BN, the EM's appear to be less anisotropic with values close to a typical semiconductor.

The differences in the electronic structures between three BN phases are better revealed in the DOS and PDOS diagrams shown in Figs. 4–6. h-BN has much narrower VB widths and much sharper band edges. This is due to the two-dimensional characteristic of the bands in a crystal with strong intralayer interaction. The bandwidths of c-BN and w-BN are similar because of similar nearest-neighbor environment (see Table I) and the same

sp^3 bonding. However, there are still some small differences in the structures in the DOS between these two phases. For example, the CB edge in *w*-BN is much sharper than in *c*-BN. These differences would be reflected more vividly in the calculated optical properties to be presented later. Another interesting point is the substantial orbital hybridization between the 2*s* and 2*p* orbitals of B and the 2*s* orbital of N. The N 2*p* states are

TABLE II. Calculated ground state and optical properties of BN.

	Cubic	Wurtzite	Hexagonal
(A) Band gap (eV):			
Indirect	5.18 ($\Gamma\rightarrow X$)	5.81 ($\Gamma\rightarrow X$)	4.07 ($H\rightarrow M$)
Direct	8.7(Γ)	8.0 (Γ)	8.9 (Γ)
	10.3 (X)	9.3 (M)	4.6 (M)
	12.4 (L)	10.7 (L)	5.6 (L)
	11.8 (K)	10.6 (A)	10.5 (A)
		12.8 (H)	4.2 (H)
		11.7 (K)	4.5 (K)
(B) Band widths (eV):			
Upper VB	10.94	11.76	10.40
VB gap	3.28	2.93	4.42
Lower VB	6.92	6.28	4.02
Total VB	21.1	21.0	18.8
(C) Effective masses (electron):			
CB edge	0.26($X\rightarrow K$)	0.24 ($K\rightarrow H$)	0.26 ($M\rightarrow\Gamma$)
	1.20 ($X\rightarrow\Gamma$)	0.35 ($K\rightarrow\Gamma$)	2.21 ($M\rightarrow L$)
VB edge	$-3.16, -0.64, -0.44$($\Gamma\rightarrow K$)	-0.88 ($\Gamma\rightarrow K$)	-0.47 ($\sim K\rightarrow\Gamma$)
	$-0.54, -0.55$($\Gamma\rightarrow X$)	-1.08 ($\Gamma\rightarrow A$)	-0.50 ($M\rightarrow\Gamma$)
	$-0.36, -1.20$($\Gamma\rightarrow L$)	-1.02 ($\Gamma\rightarrow M$)	-1.33 ($M\rightarrow L$)
(D) Effective charges (electrons):			
By Mulliken: B	2.80	2.99	2.70
N	5.20	5.01	5.30
By integration:			
B sphere:			
Radius (Å)	0.403	0.402	0.394
% of vol.	2.32	2.33	1.42
Charge	0.20	0.20	0.19
N sphere:			
Radius (Å)	0.986	0.989	0.984
% of vol.	34.0	34.7	22.3
Charge	6.4	6.0	6.7
Open region:			
% of vol.	63.7	63.0	76.3
Charge	1.40	1.80	1.11
(E) Total energy results:			
E (a.u./BN)	-12.71226	-12.70107	-12.76375
$V_{\min}/V_{\text{expt}}$	1.010	0.994	0.988
B (mbar)	3.70	3.90	3.35
B'	3.80	6.30	2.48
E_{coh} (eV)	14.00		
(F) Optical properties:			
$\epsilon(0)$	3.86	4.17	3.61
$\epsilon_{\perp}(0)$		4.16	4.32
$\epsilon_{\parallel}(0)$		4.18	2.21
Major plasmon peaks (eV)	27.3	26.4	6.9
	32.5	32.6	11.6
	38.5		23.7
			36.3

mainly confined to the upper VB. In oxides, the O 2*s* states are more localized with little interaction with other orbitals.[49]

The main band-structure results discussed above are summarized in Table II. Although there are significant differences in the published band structures of BN in earlier days, the results of more rigorous calculations in recent years agree quite well. The present band results are almost identical to those presented by Lam, Wentzcovitch, and Cohen using the first-principles pseudopotential method.[35]

B. Charge distributions

Distribution of valence electron charge in a crystal is an important aspect of the electronic structure since it reveals the bonding pattern of the crystal. The concept of effective charge Q^* on each atom or ion is useful in the empirical type of studies. However, the actual calculation of Q^* is less straightforward except in crystals of simple geometry and homopolar bonding. With a LCAO type of basis, it has been customary to use the Mulliken population analysis[53] to obtain Q^*. For systems in which the atomic wave functions are relatively localized, Mulliken analysis is a reliable prescription to obtain reasonably accurate Q^*. A more accurate approach is to use direct space integration of the charge distribution over the effective volume of the atom. However, the way in which the effective volume of the atom is determined has an element of arbitrariness itself.

We have studied the valence electron charge distribution in the three BN crystals from the self-consistent LDA calculations. In Fig. 7, the valence charge along a BN bond of 1.44 Å in *h*-BN is plotted and the charge contour map on the basal plane of the hexagonal cell is shown in the inset. Similar charge diagrams for *c*-BN and *w*-BN are shown in Figs. 8 and 9, respectively. It is clear from Fig. 7 that most valence charge in *h*-BN is around the N atom with a substantial charge in the bond region so that a precise boundary separating B and N is difficult to locate. The contour map shows the charges around both B and N atoms are not spherically distributed in the outer region because of the in-plane sp^2 bond

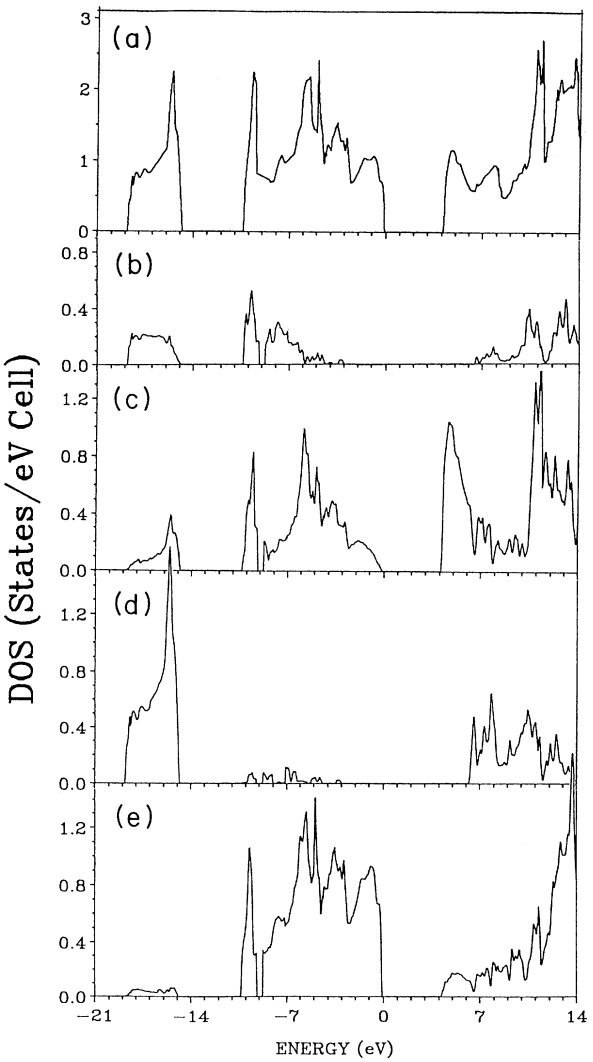

FIG. 4. Calculated DOS and PDOS of hexagonal BN: (a) Total; (b) B 2*s*; (c) B 2*p*; (d) N 2*s*; (e) N 2*p*.

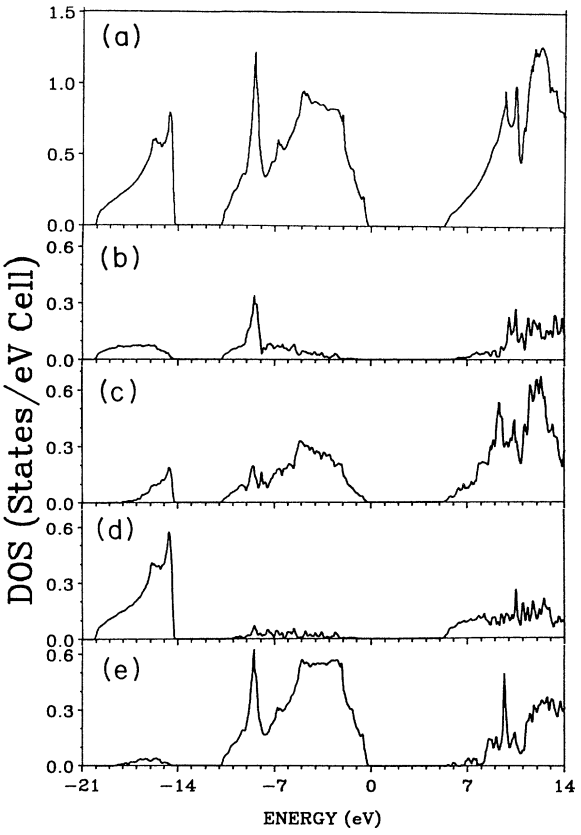

FIG. 5. Calculated DOS and PDOS of cubic BN: (a) Total; (b) B 2*s*; (c) B 2*p*; (d) N 2*s*; (e) N 2*p*.

hybridization. In the c-BN and w-BN, the BN bond lengths are slightly longer, 1.565 and 1.575 Å, respectively. In this case, the buildup of the covalent charge in the bond region is more evident.

The calculated Q^* for the three crystals are listed in Table II. The Q^* calculated with the Mulliken scheme show only a small charge transfer from B to N in h-BN and c-BN and none in w-BN. In the direct-space integration approach, we have used the effective radii for each atom as listed in Table II, by inspecting the contour maps and are therefore somewhat arbitrary. The crystal volume is then divided into three regions: the B sphere, the N sphere, and the interstitial or the bond region. The charges in each region for the three crystals are listed in Table II. As can be seen, about 14–23 % of the valence charges can be considered in the bond or interstitial region which are counted as the B charge in using the Mul-

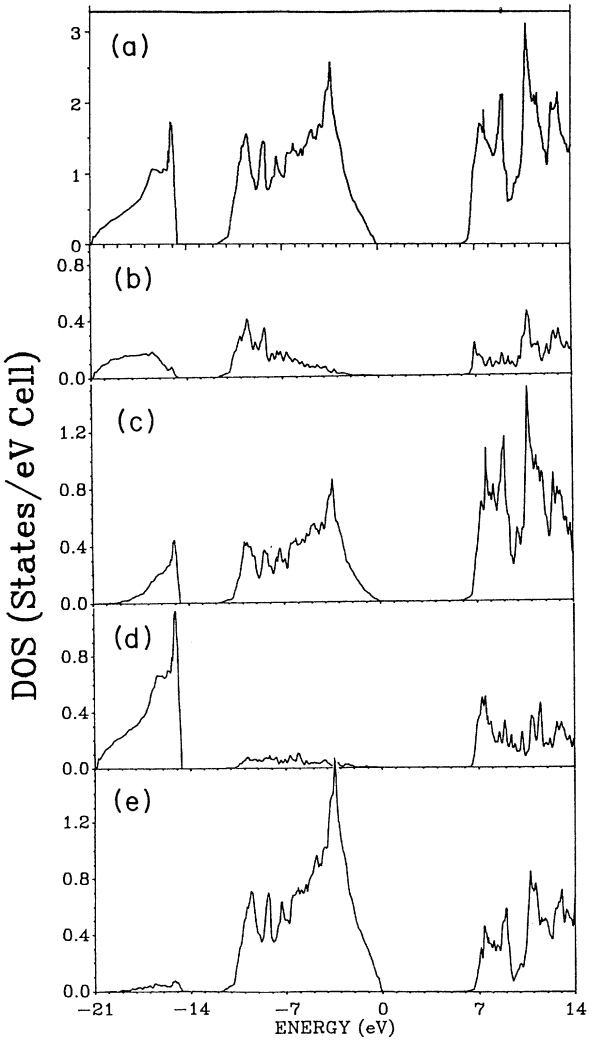

FIG. 6. Calculated DOS and PDOS of wurtzite BN: (a) Total; (b) B 2s; (c) B 2p; (d) N 2s; (e) N 2p.

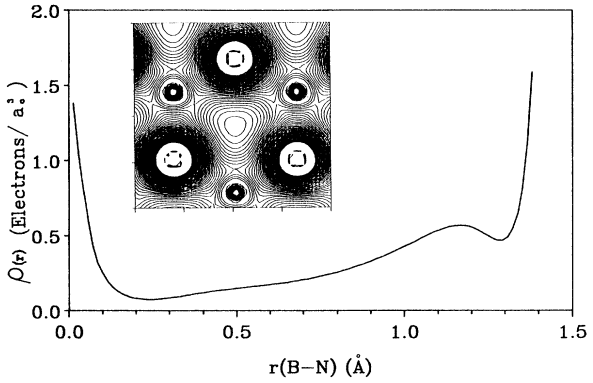

FIG. 7. Valence charge density along a short intraplane B—N bond in h-BN. Inset: contour distribution on the basal plane. The contour lines are from 0.1 to 0.25 in interval of 0.005 [in units of electron/(a.u.)^3].

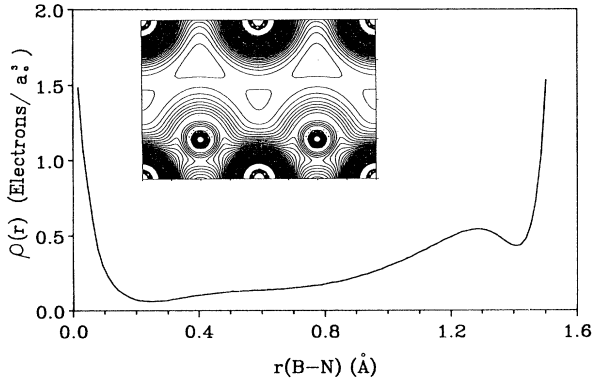

FIG. 8. Valence charge density along the B—N bond in c-BN. Inset: contour distribution on the [110] plane. Contour unit is same as Fig. 7.

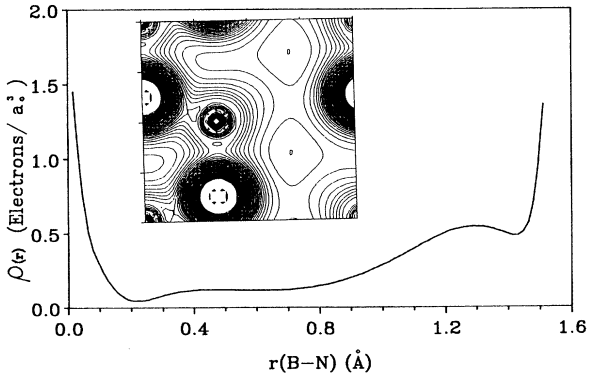

FIG. 9. Valence charge density along a vertical BN bond in w-BN. Inset: contour distribution on the {100] plane. Contour unit is the same as Fig. 7.

liken scheme. Both methods of calculating Q^* suggest the BN crystal to be highly covalent.

C. Total-energy calculation

Wentzcovitch, Cohen, and Lam had studied the TE of BN as a function of volume V for the high pressure phases of c-BN and w-BN as well as BN in rock salt and β-tin structures,[31] but not the low density h-BN. Instead, the possible transformation paths from h-BN to w-BN and from r-BN to c-BN were investigated.[32,35] Van Camp, Van Doren, and Devreese have also used the pseudopotential method for TE calculation on c-BN and demonstrated that an increase in the number of plane waves in the basis set leads to an increased accuracy in the calculated bulk properties.[33]

We have calculated the TE's of h-, c-, and w-BN as a function of crystal volume using the OLCAO method within the LDA. The results are shown in Fig. 10. We find the TE and the subsequent ground-state properties to be very sensitive to the numerical accuracy in the charge-density representation. We have sufficiently optimized the fitting function for the charge density at each calculation so as to obtain an estimated accuracy of about 0.001 a.u. per BN molecule. This accuracy enables us to compare the TE's of the three BN phases on equal footing. Our calculation shows that at the zero temperature, h-BN has the lowest TE. The h-BN which is stable at ambient conditions has an equilibrium volume $V_{\min}$ per BN molecule much higher than that of c-BN. w-BN has a $V_{\min}$ slightly smaller and an equilibrium energy $E_{\min}$ higher than c-BN. Wentzcovitch, Cohen, and Lam had also found the w-BN to have a higher $E_{\min}$ than c-BN. However, the difference in $E_{\min}$ in their calculation is about a factor of 5 smaller than our result.[31] Our calculated $V_{\min}$ for all three phases are in excellent agreement with the measured values listed in Table I with a maximum deviation of only about 1%.

From the E vs V curves fitted to the Murnagan equation of state,[54] we obtain the bulk modulus B and the pressure coefficients B' which are listed in Table II. Hexagonal BN has a bulk modulus of 3.35 Mbar, considerably smaller than the 3.70 Mbar for c-BN and 3.92 Mbar for the w-BN. This is in excellent agreement with the measured values of $B=3.69$ Mbar and $B'=4.0\pm0.2$ for c-BN.[36] We have also obtained a cohesive energy of 14.0 eV per BN for c-BN which is somewhat higher than the estimated value of 13.2 eV.[35] A 6% overestimation of the cohesive energy is a rather common feature with LDA calculations.

If we only consider the static lattice, i.e., if the effect of zero-point energy and lattice vibrations at finite temperature are ignored, we may explore the possible phase transitions from the TE curves. In Fig. 10, from the tangent drawn on the E-V curves, we have estimated the transition pressure from the c-BN to w-BN to be 1.33 Mbar occurring at a volume of about 80% of V_0, the measured $V_{\min}$ of c-BN. These values are in reasonable agreement with the experimental measurement of Knittle *et al.*[36] In Fig. 11, we display the P-V curve for the c-BN together with the experimental data[36] and the result of Van Camp, Van Doren, and Devreese.[33] Both the calculations are in good agreement with the measured data.

A similar transition tangent from h-BN to c-BN can also be drawn as shown in Fig. 10 by a dotted line. The slope of this tangent gives a "transition" pressure of only

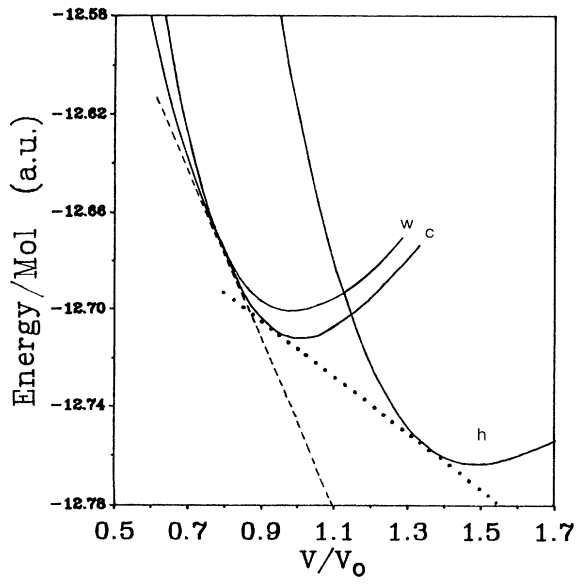

FIG. 10. Calculated total energies per BN molecule as a function of volume for three phases of BN: (a) cubic, (b) hexagonal, and (c) wurtzite. V_0 is the measured equilibrium volume of cubic BN. The dashed line shows possible transition from c-BN to w-BN and the dotted line shows possible transition from h-BN to c-BN.

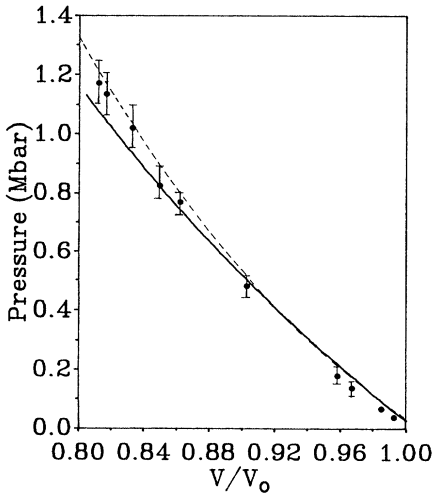

FIG. 11. Calculated P vs V for c-BN. The dotted line is theoretical calculation of Ref. 33 and the data points are from measurements of Ref. 36.

0.43 Mbar and a transition volume of $0.94V_0$ on the c-BN side and $1.37V_0$ on the h-BN side. However, it is not at all clear that such a phase transition may actually occur. Wentzcovitch *et al.* had shown that transition to c-BN is more likely from the r-BN while that to w-BN is from the h-BN because of the difference in the stacking sequence of the layer structure. Transition path calculation shows an energy barrier along the pathway. They did not specify the lattice parameters use in their calculation, and it is not clear if they have used the same lattice parameters as those listed in Table I. Although our TE calculation with BN gives results in good agreement with other published results, we did not attempt to achieve ultrahigh accuracy by optimizing all the computational intricacies in order to perform additional calculations such as the frequency of a specific phonon mode for several reasons. First, the work of Refs. 30–32 and Van Camp, Van Doren, and Devreese[33] were rather complete in the study of the equation of states and the energetic associated with the phase transformation. It is unlikely that, within the general LDA theory, a better result can be obtained. Second, to achieve an accuracy in TE of better than 0.01 eV per molecule will require substantially more computer resources. Third, we intend to focus more on the optical properties of BN in this paper.

III. OPTICAL PROPERTIES

There have been several past optical[55–60] and energy-loss[61,62] measurements on h-BN. Early data were very conflicting in nature mostly because of poor samples. Band structures calculated at that time were not accurate enough to be of any help. Very recently, careful measurement of inelastic-electron-scattering spectra on well-characterized h-BN samples became available.[39] The optical dielectric constants and other properties can be extracted from the energy-loss spectra and analyzed. At about the same time, the optical constants on single-crystal c-BN in the vacuum ultraviolet (vuv) region were reported.[40] Ellipsometry measurements have also been used to characterize the noncrystalline thin films of BN (Refs. 10 and 39) and reflectance spectra of c-BN films have been published.[9] The interpretation of these data can be facilitated by accurate band-structure and optical-absorption calculations which have been very successfully carried out on a variety of complex crystals.[46–52] We find no optical data on w-BN, and we hope our calculations on all three phases of BN will lead to further experimental efforts on BN crystals and thin films. By combining the measured data with the calculation, a near total understanding of the electronic and optical properties of BN is possible.

The specific method and procedures for the optical calculation using the OLCAO method have been discussed before.[41] The calculation is based on the band results discussed in the preceding section. The momentum matrix elements (MME) associated with dipole transition are evaluated explicitly at a large number of **k** points in the BZ. To have a general overview of the optical properties of the three BN crystals, we first display the calculated interband optical conductivities σ (averaged over the three crystallographic directions in Fig. 12). Also shown are the joint DOS (JDOS). The JDOS would be proportional to σ when the effect of **k** dependence of the MME is ignored and has frequently been used as a simple way of explaining the absorption data. In Fig. 12, we set the arbitrary units for the JDOS to be such that they match with the σ curve in the threshold region. Several facts become apparent: First, the σ of the three phases of BN are very different; not only with the layer-structure h-BN, but also between the tetrahedrally coordinated c-BN and w-BN where the bonding is supposed to be much closer. Second, the absorption threshold and the strength in h-BN are much smaller than that of c-BN or w-BN. The calculated transition threshold reflects the minimal direct band gap (the separation of the top of the VB and the bottom of the CB at the same **k**). All three crystals have indirect band gaps as discussed before. But in h-BN, the indirect band gap is smaller than those of c-BN or w-BN, and is also very close to the direct gap because of the two-dimensional characteristic of the bands. This leads to a much lower absorption threshold in h-BN. There has been much controversy as to whether the gap in h-

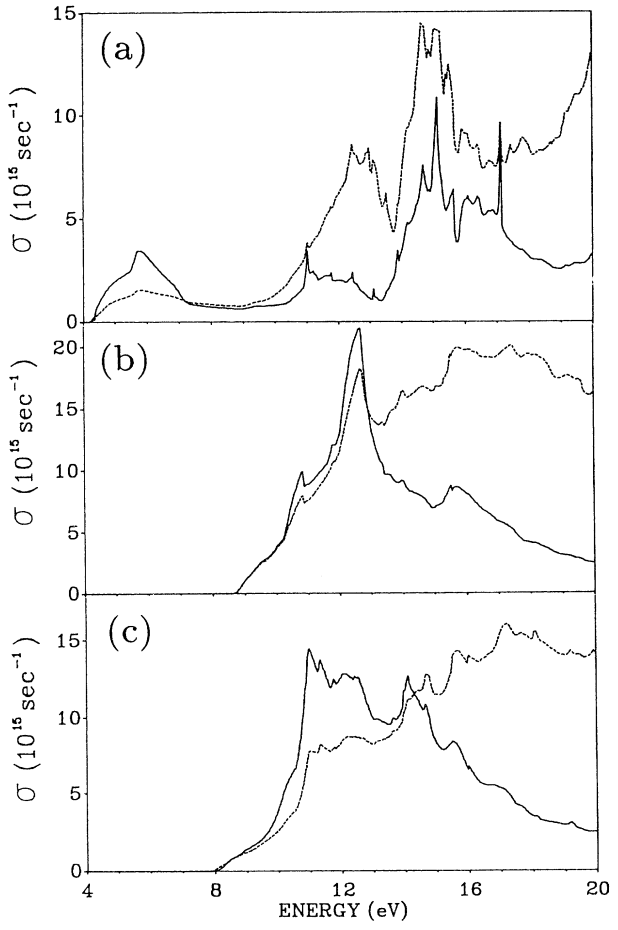

FIG. 12. Calculated interband optical conductivity $\sigma(\omega)$ (solid line) and the joint DOS (dashed line) for (a) h-BN; (b) c-BN; (c) w-BN. The JDOS's are in arbitrary units.

BN is direct or indirect in the earlier optical measurements. The present calculation shows that this is not an important issue. Assuming the phonon-assisted transitions in BN are negligible, then the optical gap would actually correspond to the minimum direct gap which, in c-BN and w-BN, is substantially larger than the indirect gap. Third, there is very little resemblance between σ and the JDOS curves especially in the high-frequency region, indicating a significant $\mathbf{k}$ dependence of the MME in all three crystals. Fourth, there are many prominent structures in the conductivity curves which could be related to the measured data for direct comparisons. Of particular interest is the leading peak centered at 5.8 eV in σ for h-BN. It turns out that this peak is due to transitions between bands in the in-plane direction (a-b) and reflects the strong anisotropy in the optical absorption in h-BN.

Let us first consider h-BN in more detail. From the inelastic-electron-scattering data at various momentum transfers, TS extracted the dielectric function for h-BN from the electron-energy-loss function (ELF) or the imaginary part of $-1/\epsilon(\omega)$.[39] By carefully studying samples of different qualities, a gap value of 5.9 eV is established. This is to be compared with our calculated indirect gap of 4.07 eV and the minimal direct gap of 4.2 eV (at H). The measured data were also resolved in directions perpendicular to the c axis ($\perp$) (in the a-b plane) and parallel ($\parallel$) to the c axis. Since the convolution of data from ELF to $\epsilon(\omega)$ may introduce additional uncertainties because of the unavoidable assumptions employed, and since the convolution of the theoretical data is more controllable, it is preferable to compare the calculated and measured ELF's which are shown in Fig. 13. There are two experimental curves from Ref. 39, one with a momentum transfer of 0.13 Å^{-1} in the a-b plane (in-plane data); the other with a momentum transfer of 0.15 Å^{-1} along the c axis (c-axis data). There is an excellent agreement between theory and experiment in regards to the general shape of the ELF and the positions of peaks within the entire 40-eV range. The calculated ELF shows peaks at 6.9, 11.6, 23.7, 29.8, and 36.3 eV and shoulderlike structures at 15.8 and 18.9 eV. The peak at 6.9 eV corresponds to the peak at 7.4 eV in the c-axis data and the peak at 8.2 eV in the in-plane data. The slight shift in the position of this peak can be explained by the underestimation of the band gap which has its root in the LDA theory. The peak at 11.6 eV corresponds to the one at 11.8 eV in the c axis data. There is no evidence in either of the data for the weak shoulder at 15.8 eV, but this could be due to the measurement at finite momentum transfer which somewhat limits the resolution. The other shoulder at 18.9 eV has evidence in both data at about the same position. The most prominent peak in the ELF is at 23.7 eV which lies between the similarly prominent peaks at 22.7 and 25.7 eV for the c-axis and in-plane data, respectively. At an even higher energy, the peak at 29.8 eV corresponds to the peak in the c-axis data at 30.5 eV. There is evidence of a weak peak in both data for the peak at 36.3 eV.

To explain the apparent anisotropy in the ELF data of Fig. 13, we plot the in-plane and z components of the cal-

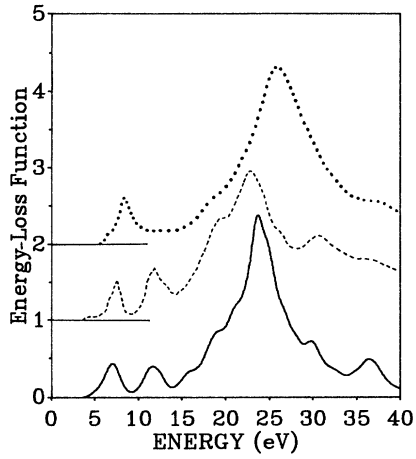

FIG. 13. Energy-loss function in h-BN: solid line, present calculation; dashed line, measurement from Ref. 39 with q along c axis; dotted line, with q in the a-b plane.

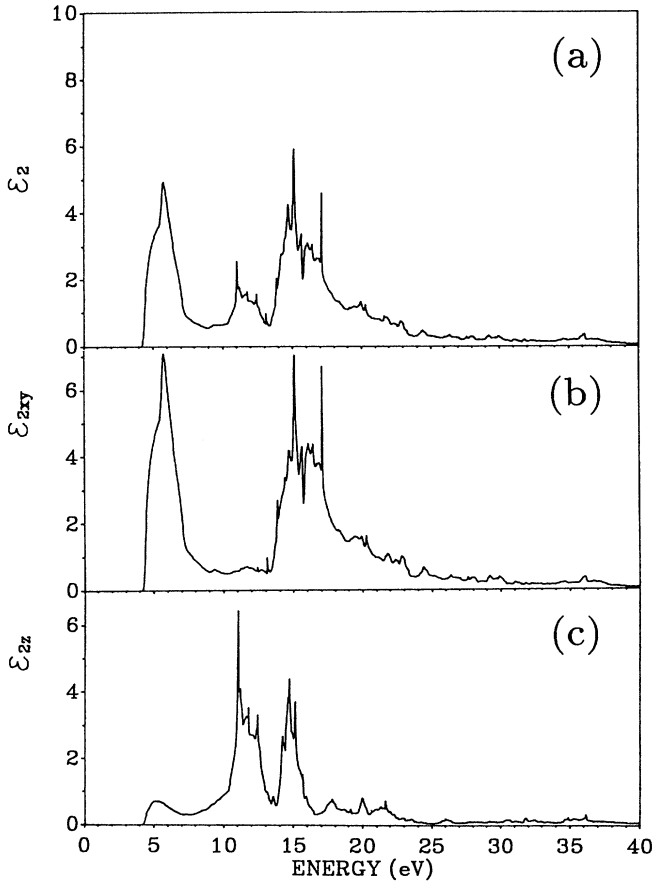

FIG. 14. Calculated dielectric function for h-BN. (a) Average over three directions; (b) average over x and y directions; (c) z component.

culated $\epsilon_2(\omega)$ from 4 to 40 eV in Fig. 14. The anisotropic behavior of $\epsilon_2(\omega)$, hence the ELF, becomes quite obvious. In particular, the peak at 11.6 eV in the ELF is definitely from the $\|$ component to the c axis. The direction-resolved $\epsilon_2(\omega)$ curves also suggest that the major peak has contributions from both components with the $\|$ component at a lower energy than the $\perp$ component, consistent with the data of Ref. 39.

In Fig. 15, we show the similar ELF for c-BN and w-BN. For c-BN, there are marked plasmon peaks at 27.3, 32.5, and 38.5 eV and less prominent features at 11.1, 15.0, and 24.4 eV. For w-BN, there are two major plasmon peaks at 26.4 and 32.6 eV with shoulderlike structures at 12.9, 23.6, 28.6, and 36.9 eV. We found one ELF datum for c-BN.[66] This is shown in Fig. 15 by a dotted line without any shift in energy scale. In spite of the low resolution, it is clear that the general shape and profile of the measured data are in good agreement with our calculation. No direct ELF data for w-BN is available for comparison. However, with the good agreement in both h-BN and c-BN, we expect our calculated ELF for w-BN to be equally accurate.

We now turn to the other optical data for the c-BN. There have been only a few previous optical measurements on c-BN.[63–65] Figure 16 shows the calculated imaginary part of the dielectric function for c-BN from 0 to 40 eV. Also shown are the data of Osaka *et al.* for c-BN in the energy range from 5 to 25 eV obtained from the reflectance spectrum by Kramers-Kronig transformation.[9] The measured data show major peaks A and B at 11.0 and 8.9 eV, a minor peak C at 16.4 eV, and a shoulderlike structure D near 12.5 eV. For easy comparison, we have aligned the positions of the central peak A in Fig. 16. There is a good overall agreement between the

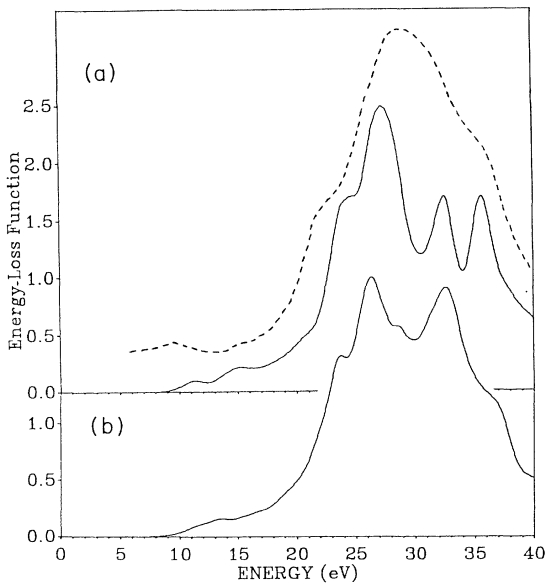

FIG. 15. Energy-loss function for (a) c-BN, the dotted line is the measured data from Ref. 66; (b) w-BN.

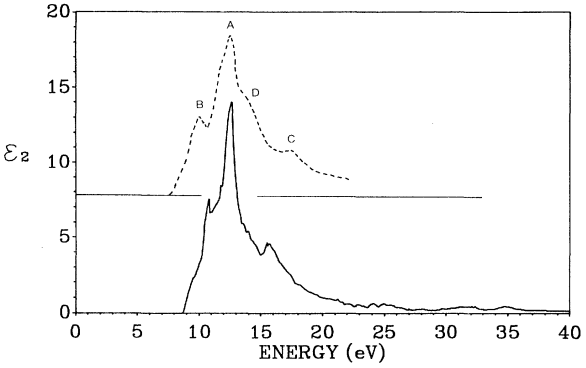

FIG. 16. Solid line: calculated $\epsilon_2(\omega)$ for c-BN; dashed line: measured data from Ref. 9 with the major peak at 11 eV aligned.

two curves with the major structures clearly identified. However, the calculated peak positions for A, B, and C are at 12.6, 10.7, and 15.6 eV, respectively, with less evidence for the shoulder D. Hence, with this set of measured data, the calculated peak positions are about 1.7 eV too high. If one accepts the notion that the LDA calculation generally underestimates the band gap, then one would expect the calculated peak positions to be at a lower rather than a higher photon energy. Apparently, the calculated direct gap in c-BN is larger than that inferred from the optical measurements, even though the calculated indirect gap is 5.18 eV. This could indicate that the accuracy for the higher CB states as calculated by the LDA theory is energy and momentum dependent. A smaller gap does not necessarily mean that higher CB's are correspondingly lower in energy. As a matter of fact, several of our recent calculations[41,47–49] on large gap insulators indicate that the major peaks in the optical-absorption curves are in good agreement with experiments, even though the calculated gap, or the absorption threshold are smaller than those measured. More accurate measurement on well-characterized single-crystal c-BN will be very useful to further clarify this point. One may ask if an even larger basis set than the present one will improve the agreement. This is not likely,[67] given the fact of the good agreement in h-BN for frequency up to 40 eV. In any case, our calculated $\epsilon_2(\omega)$ is in much better agreement with experiment than the earlier calculation by Tsay, Vaidyanathan, and Mistra using empirical pseudopotential method.[24]

Miyata and Moriki has also measured the refluctance and transmittance spectra on single-crystal c-BN in the vuv and determined the fundamental absorption edge to be at 6.1 eV.[40] However, their converted absorption coefficient is quite different from our σ curve shown in Fig. 12(b) and the data of Osaka *et al.*[9] shown in Fig. 16 at photon energies above 15 eV. In Fig. 17, we make a direct comparison of the refractive index data with the calculated one from $n(\omega)=\sqrt{\epsilon(\omega)}$. As can be seen, there is a reasonable overall agreement. This may indicate that

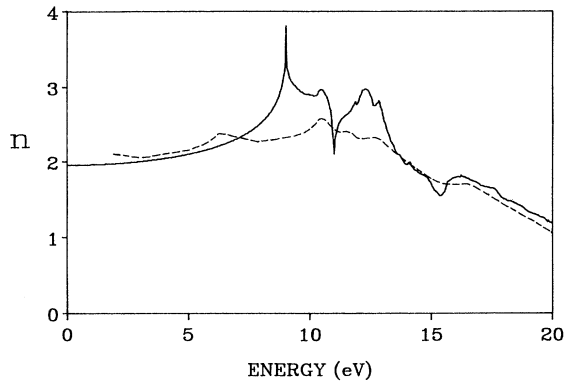

FIG. 17. Refractive index n for c-BN: Solid line, present calculation; dashed line, experimental data from Ref. 40.

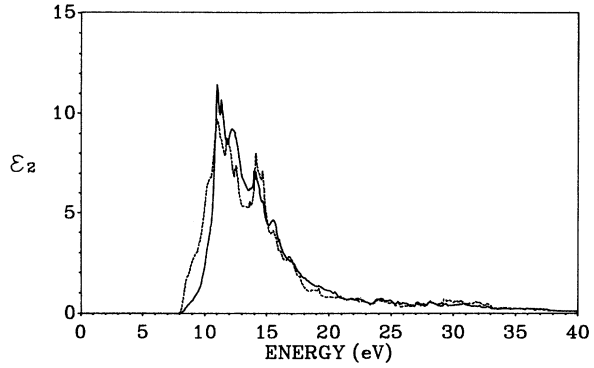

FIG. 18. Calculated dielectric function for w-BN: solid line, $\epsilon_2^{\perp}(\omega)$; average over x-y directions; dashed line, $\epsilon_2^{\parallel}(\omega)$.

the formulas used by Miyata and Moriki for the phase change on the reflection are not quite valid in high photon energy range.[40]

There are no reported optical data on w-BN mainly because it is formed only at a very high pressure and temperature. In Fig. 18, we show the calculated $\epsilon_2(\omega)$ curves in the $\parallel$ (z component) and $\perp$ (average over x and y directions) components of the hexagonal wurtzite lattice. The main peak is at 10.9 eV and there is less anisotropy than in h-BN. Near the absorption edge, the z component of $\epsilon_2(\omega)$ has a much higher absorption than the in-plane component. We hope our calculation will stimulate future optical measurement on w-BN.

The zero-frequency limit of the dielectric function $\epsilon(0)$, is an important physical quantity. The calculated values (averaged over three directions) for h-, c-, and w-BN are 3.86, 4.32, and 4.16, respectively. They are generally close but smaller than the experimentally determined values.[66,68] The small discrepancy can be attributed to the difference in the calculated and the measured band gap. For h-BN, the $\parallel$ component of $\epsilon(0)$ is smaller than the $\perp$ component, in qualitative agreement with the values deduced from the reflection spectra in the infrared region.[68] The calculated $\epsilon(0)$ values together with the major plasmon peaks in the three crystals are listed in Table II.

IV. DISCUSSION AND CONCLUSIONS

We have studied the ground state and the optical properties of three phases of BN using the OLCAO method. For the ground-state properties, our results are in good agreement with experiments and other recent calculations. We may conclude that the basic electronic structures for the three different phases of BN are reasonably established.

Our total-energy calculations on BN give results in close agreement with the pseudopotential calculations. This again demonstrates the effectiveness of the OLCAO method in the study of structural phase transitions in crystals via first-principles TE calculations. The accuracy in the TE calculation may be further improved if other optimization procedures to minimize errors are employed.

The calculation on the optical properties is most enlightening. The excellent agreement between our calculation and the inelastic-electron-scattering measurement for the h-BN gives credence to the results on the other two phases on which reliable data are still lacking. It is also demonstrated that the accuracy of CB states in insulators such as BN is energy and momentum dependent, and is best assessed by the calculated optical spectra in comparison with the measured data. It may be an oversimplification to just compare the gap size from the LDA calculation with the one deduced from the optical data, because the latter may be complicated by the dominance of the direct transitions and, to a certain extent, depends on the extrapolation procedure near the threshold where the signal would be quite weak.

ACKNOWLEDGMENT

This work is supported by the Department of Energy under Grant No. DE-FG02-84ER45170.

[1] *Synthesis and Properties of Boron Nitride,* edited by J. J. Pouch and S. A. Alteroviz (Trans Tech, Aedermannsdorf, Switzerland, 1990).

[2] *Numerical Data and Functional Relationship in Science and Technology—Crystal and Solid State Physics,* edited by O. Madelung, Landolt-Börnstein Vol. III (Springer, Berlin, 1972).

[3] R. S. Pease, Acta Crystallogr. **5** 536 (1952).

[4] R. H. Wentorf, J. Chem. Phys. **38**, 1144 (1957).

[5] F. P. Bundy and R. H. Wentorf, J. Chem. Phys. **38**, 1144 (1963).

[6] T. Soma, A. Sawaoka, and S. Saito, Mater. Res. Bull. **7**, 755 (1974).

[7] T. Sato, T. Ishii, and N. Setaka, J. Am. Ceram. Soc. C **162**, (1982).

[8] See, for example, several articles in *Synthesis and Properties of*

Boron Nitride (Ref. 1).
[9]Y. Osaka, A. Chayahara, H. Yokoyama, M. Okamoto, T. Hamada, and M. Fujisawa, in *Synthesis and Properties of Boron Nitride* (Ref. 1), pp. 227–297.
[10]C. R. Aita, in *Synthesis and Properties of Boron Nitride* (Ref. 1), pp. 1–20.
[11]L. Kleinman and J. C. Phillips, Phys. Rev. **117**, 460 (1960).
[12]D. Stoker, Proc. R. Soc. London **270**, 397 (1962).
[13]F. Bassani and M. Yoshimine Phys. Rev. **130**, 20 (1963).
[14]D. R. Wiff and R. Keown, J. Chem. Phys. **47**, 3133 (1967).
[15]J. C. Phillips, J. Chem. Phys. **48**, 5740 (1968).
[16]E. Doni and G. Pastori Parravicini, Nuovo Cimento B **64**, 117 (1969).
[17]M. S. Nakhmanson and V. P. Smirnov, Sov. Phys.—Solid State **13**, 2763 (1971).
[18]J. Zupan, Phys. Rev. B **6**, 2477 (1972); J. Zupan and D. Koler, J. Phys. C **5**, 3097 (1972).
[19]L. A. Hemstreet and C. Y. Fong, Phys. Rev. B **6**, 1464 (1972).
[20]A. Zunger, A. Katzir, and A. Halperin, Phys. Rev. B **13**, 5560 (1976).
[21]B. M. Davies, F. Bassani, F. C. Brown, and C. G. Olson, Phys. Rev. B **24**, 3537 (1976).
[22]H. C. Hwang and J. Henkel, Phys. Rev. B **17**, 4100 (1978).
[23]A. Zunger and A. J. Freeman, Phys. Rev. B **17**, 2030 (1978).
[24]Y. F. Tsay, A. Vaidyanathan, and S. S. Mistra, Phys. Rev. B **19**, 5422 (1979).
[25]R. Dovesi, C. Pisani, and C. Roetti, Int. J. Quantum Chem. **17**, 517 (1980).
[26]J. Roberson, Phys. Rev. B **29**, 2131 (1984).
[27]M. Z. Huang and W. Y. Ching, J. Phys. Chem. Solids **46**, 977 (1985).
[28]K. T. Park, K. Terakura, and N. Hamada, J. Phys. C **20**, 1241 (1987).
[29]Z. Catellani, M. Posternak, A. Balderreschi, and A. J. Freeman, Phys. Rev. B **36**, 6105 (1987).
[30]R. M. Wentzcovitch, K. J. Chang, and M. L. Cohen, Phys. Rev. B **34**, 1071 (1986).
[31]R. M. Wentzcovitch, M. L. Cohen, and P. K. Lam, Phys. Rev. B **36**, 6058 (1987).
[32]R. M. Wentzcovitch, S. Fahy, Marvin L. Cohen, and S. G. Louie, Phys. Rev. B **38**, 6191 (1988).
[33]P. E. Van Camp, V. E. Van Doren, and J. T. Devreese, Solid State Commun. **71**, 1055 (1989).
[34]E. K. Takahashi, A. T. Lino, A. C. Ferranz, and J. R. Leite, Phys. Rev. B **41**, 1691 (1990).
[35]P. K. Lam, R. M. Wentzcovitch, and M. L. Cohen, in *Synthesis and Properties of Boron Nitride* (Ref. 1), pp. 165–192.
[36]E. Knittle, R. M. Wentzcovitch, R. Jeanloy, and M. L. Cohen, Nature (London) **337**, 349 (1989).
[37]S. K. Estreicher, C. H. Chu, and D. S. Marynick, Phys. Rev. B **40**, 5739 (1989).
[38]For a detailed account of earlier experiments on *h*-BN, see Ref. 29 and the references cited therein.
[39]C. Tarrio and S. E. Schnatterly, Phys. Rev. B **40**, 7852 (1989).
[40]N. Miyata and K. Moriki, Phys. Rev. B **40**, 12 028 (1989).
[41]W. Y. Ching, J. Am. Ceram. Soc. **73**, 3135 (1990).
[42]B. N. Harmon, W. Weber, and D. R. Hamann, Phys. Rev. B **25**, 1109 (1982).
[43]F. Zandiehnadem and W. Y. Ching, Phys. Rev. B **41**, 12 162 (1990).
[44]W. Y. Ching and B. N. Harmon, Phys. Rev. B **34**, 5305 (1986).
[45]Y.-N. Xu and W. Y. Ching, in *SiO2 and Its Interfaces,* edited by S. T. Pantelides and G. Lucovsky, MRS Symposia Proceedings No. 105 (Materials Research Society, Pittsburgh, 1988), p. 181.
[46]W. Y. Ching, Y. N. Xu, and K. W. Wong, Phys. Rev. B **40**, 8111 (1989).
[47]Y.-N. Xu and W. Y. Ching, Phys. Rev. B **41**, 5471 (1990).
[48]W. Y. Ching and Y.-N. Xu, Phys. Rev. Lett. **65**, 891 (1990).
[49]Y.-N. Xu and W.-Y. Ching, Phys. Rev. B **43**, 4463 (1991).
[50]J. C. Parker, U. W. Gelser, D. J. Lam, Y.-N. Xu, and W. Y. Ching, J. Phys. Am. Ceram. Soc. **71**, 3206 (1990).
[51]J. C. Parker, D. J. Lam, Y.-N. Xu, and W. Y. Ching, Phys. Rev. B **42**, 5489 (1990).
[52]Y.-N. Xu, W. Y. Ching, and R. H. French, Ferroelectrics **111**, 23 (1990).
[53]R. S. Mulliken, J. Am. Chem. Soc. **77**, 887 (1954).
[54]F. D. Murnagan, Proc. Natl. Acad. Sci. U.S.A. **30**, 244 (1944).
[55]M. J. Rand and J. F. Roberts, J. Electrochem. Soc. **115**, 423 (1968).
[56]W. Baronian, Mater. Res. Bull. **7**, 119 (1972).
[57]J. Zupan and D. Kolar, J. Phys. C **5**, 3097 (1972).
[58]A. Zunger, A. Katzir, and A. Halperin, Phys. Rev. B **13**, 5560 (1976).
[59]R. Mamy, J. Thomas, G. Jezequel, and J. C. Lemonnier, J. Phys. (Paris) Lett. **42**, L473 (1981).
[60]D. Hoffman, G. L. Doll, and P. C. Eklund, Phys. Rev. B **30**, 6051 (1984).
[61]U. Buchner, Phys. Status Solidi B **81**, 227 (1977).
[62]R. D. Leapman, P. L. Fejes, and J. Silcox, Phys. Rev. B **28**, 2361 (1983).
[63]H. R. Philipp and E. A. Taft, Phys. Rev. **127**, 1157 (1962).
[64]R. M. Chrenko, Solid State Commun. **14**, 511 (1974).
[65]V. A. Formichev and M. A. Rumsch, J. Phys. Chem. Solids **29**, 1015 (1968).
[66]D. R. McKenzie, W. G. Sainty, and D. Green, in *Synthesis and Properties of Boron Nitride* (Ref. 1), p. 193.
[67]Our recent calculation on large gap insulator CaF_2 indicates that further augmentation of basis set beyond the present full basis does not change the optical-absorption curve up to at least 25 eV.
[68]R. Geick, C. H. Perry, and G. Rupprecht, Phys. Rev. **146**, 543 (1966)